JACS
JOURNAL OF THE AMERICAN CHEMICAL SOCIETY
Article
pubs.acs.org/JACS

Hexagons to Ribbons: Flipping Cyanide on Au{111}

Andrew I. Guttentag,[†,‡] Kristopher K. Barr,[†,‡] Tze-Bin Song,[†,§] Kevin V. Bui,[∥,⊥] Jacob N. Fauman,[∥,#] Leticia F. Torres,[∥,⊗] David D. Kes,[∥,▽] Adina Ciomaga,[×] Jérôme Gilles,[◇] Nichole F. Sullivan,[¶] Yang Yang,[†,§] David L. Allara,[*,¶] Michael Zharnikov,[*,○] and Paul S. Weiss[*,†,‡,§]

[†]California NanoSystems Institute, University of California, Los Angeles, Los Angeles, California 90095, United States
[‡]Department of Chemistry and Biochemistry, University of California, Los Angeles, Los Angeles, California 90095, United States
[§]Department of Material Science and Engineering, University of California, Los Angeles, Los Angeles, California 90095, United States
[∥]Department of Mathematics, University of California, Los Angeles, Los Angeles, California 90095, United States
[⊥]Department of Industrial Engineering and Management Sciences, Northwestern University, Evanston, Illinois 60208, United States
[#]Department of Physics, University of California, Santa Barbara, California 93106, United States
[⊗]Department of Mathematics, University of San Francisco, San Francisco, California 94117, United States
[▽]Department of Mathematics and Natural Sciences, California State University, Long Beach, California 90840, United States
[×]Department of Mathematics, Laboratoire Jacques Louis Lions, Université Paris Diderot, 5 Rue Thomas Mann, Paris 75013, France
[◇]Department of Mathematics and Statistics, San Diego State University, San Diego, California 92182, United States
[¶]Department of Chemistry, Pennsylvania State University, University Park, Pennsylvania 16802, United States
[○]Applied Physical Chemistry, Heidelberg University, 69120 Heidelberg, Germany

Supporting Information

ABSTRACT: Cyanide monolayers on Au{111} restructure from a hexagonal close-packed lattice to a mixed-orientation "ribbon" structure through thermal annealing. The new surface structure loses most of the observed surface features characterizing the initial as-adsorbed system with "ribbon" domain boundaries isolating rotationally offset surface regions where the orientation is guided by the underlying gold lattice. A blue shift to higher frequencies of the CN vibration to 2235 cm^{-1} with respect to the as-adsorbed CN/Au{111} vibration at 2146 cm^{-1} is observed. In addition, a new low-frequency mode is observed at 145 cm^{-1}, suggesting a chemical environment change similar to gold−cyanide crystallization. We discuss this new structure with respect to a mixed cyanide/isocyanide monolayer and propose a bonding scheme consisting of Au-CN and Au-NC bound molecules that are oriented normal to the Au{111} surface.

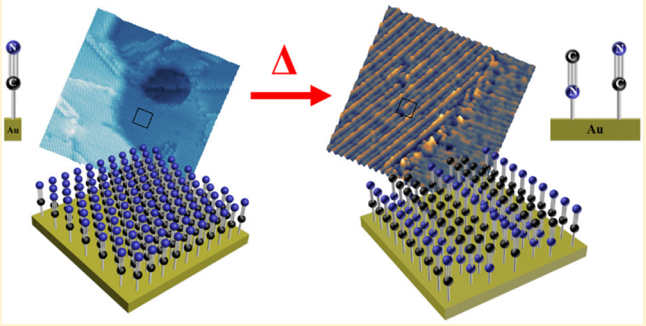

INTRODUCTION

Directing the self-organization of molecular systems requires understanding the effects of changing basic parameters and external stimuli, such as temperature, electrical potential, and illumination, on molecular and intermolecular structure and function.[1−5] Self-assembled monolayers (SAMs) are a common system in which to test these effects, which can result in both physical and chemical changes.[6−9] Similar to thiols and selenols, carbon-bound molecules have been shown to form ordered monolayers on gold substrates.[10−14] The strength of the Au−C bond is similar to that of Au−S and Au−Se bonds.[13,14] There is significant interest in understanding how temperature affects the organization,[6,15−17] conductivity,[17] adsorption,[18] stability,[13,19] and molecular reactivity[20] of SAMs, as those properties are critical in effectively tailoring molecular design for research and applications in nanotechnology.[4,21,22]

Monolayer structures can be elucidated through vibrational spectroscopy,[10,23−26] molecular-resolution imaging,[27−30] and complementary techniques. Even relatively small shifts of vibration peaks can be sources of significant information pertaining to the morphology,[24,31] structure,[10,32−35] composition, and defects of SAMs.[24,36,37] To this end, we have fabricated and probed the vibrational spectra and structures of monolayers of cyanide molecules on Au{111}.[7,38] In this work, we report the structure and orientation for annealed cyanide monolayers on Au{111}, report changes in the vibrational spectra, and propose mixed bonding schemes to explain the appearance of "ribbons" consisting of rows of cyanide molecules.

Received: June 12, 2016
Published: November 7, 2016

ACS Publications © 2016 American Chemical Society

DOI: 10.1021/jacs.6b06046
J. Am. Chem. Soc. 2016, 138, 15580−15586

Initially, cyanide molecules deposited at room temperature assemble on Au{111} in a hexagonal close-packed (hcp) lattice attached through the carbon atom, oriented primarily normal to the surface.[38] Cyanide has a strong dipole moment, 2.8 D, that makes it ideal as a small-molecule probe.[39,40] In our previous work we adsorbed cyanogen (C_2N_2) on Au{111}, but it did not dissociate under the conditions used.[41] Here, we were able to deposit CN on Au{111} and to induce a structural change upon a simple dry thermal annealing process.

RESULTS AND DISCUSSION

Surface Structure Characterization of Thermally Annealed CN/Au{111}. Cyanide molecules deposited on Au{111} from exposure to HCN(g) under atmospheric conditions order in a hcp lattice at room temperature.[38] Figure 1A shows the structural details of cyanide monolayers, obtained

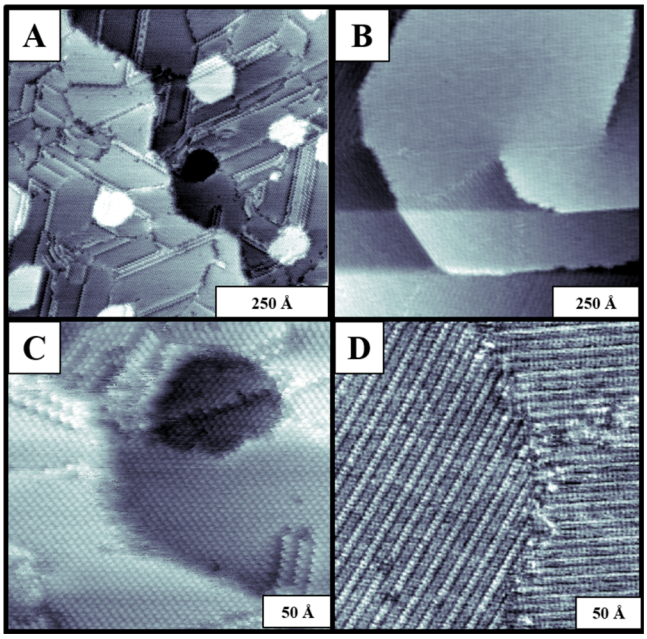

Figure 1. Scanning tunneling microscope images of (A) hexagonally close-packed CN/Au{111} as-deposited under ambient conditions and (B) the thermally induced ribbon structure formed by dry annealing for over 18 h at ∼100 °C. The order in the annealed structure is long range (on the order of tens of nanometers) with the ribbon domains taking on various rotational orientations relative to one another on the surface. Once annealed, the surface never returns to the original hcp arrangement. (C,D) Molecular-resolution images of the as-adsorbed and thermally annealed lattices, respectively. We note tip-change imaging artifacts in (B) that did not disrupt the topography. Imaging conditions: V_{sample} = −1 V and I_{tunnel} = 5 pA.

under ambient conditions by scanning tunneling microscopy (STM), which include surface features such as vacancy islands, protruding islands, and multiple highly ordered domains. In this cyanide-on-Au{111} structure, the measured nearest-neighbor spacing is 3.8 ± 0.5 Å.[38]

After as-adsorbed CN/Au{111} samples were heated to 100 °C for over 18 h, the original surface features were completely replaced, as shown in Figure 1B, with ribbon-like structural domains that are typically larger, spanning tens to hundreds of nanometers, than those observed prior to thermal annealing, which are on the order of 1−10 nm. Closer inspection of the surface structure reveals the changes at the molecular level from the initial CN/Au{111} hcp lattice, shown in Figure 1C, to the new ribbon arrangement, shown in Figure 1D. Two common defects found in the ribbon system are highlighted in Figure 1D: molecular-level disruptions of the individual ribbon "stripes" and domain boundaries between regions of different surface orientation. Once converted, the ribbon structure has not been observed to return to the hcp lattice and has been stable for imaging for several months under standard storage conditions (i.e., in a dark, dry, sealed container).

Annealing up to 60 °C for over 18 h induced no observable change in the as-adsorbed CN/Au{111} hcp lattice, while annealing to 100 ± 5 °C induced ribbon formation, typically to completion. Using this same temperature window, both structures are observed coexisting on the surface after 6 h, as in Figure 2A. Single-molecule resolution imaging of this system

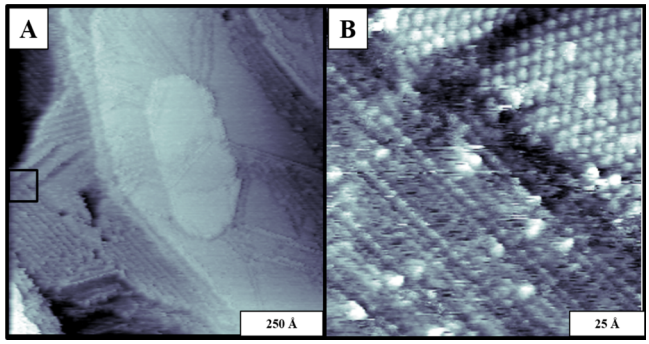

Figure 2. (A) Transition from hcp to ribbon structure imaged after 6 h exposure to ∼100 °C. (B) Higher resolution image, highlighting a region with both (upper right) hexagonally close-packed and (lower left) ribbon structure regions. Imaging conditions: V_{sample} = −1 V and I_{tunnel} = 5 pA.

with STM, in Figure 2B, shows both the hcp lattice (in the top right corner) and the emergence of the ribbon region (in the bottom left), with isolated molecule features appearing in both regions that are not part of the respective lattices. Importantly, annealing for over 18 h does not affect the ribbon structure; annealing periods of 24 h were typically used to ensure complete conversion. However, annealing at temperatures above 105 °C for 18−24 h generally results in deterioration of the sample. This observation agrees with the established temperature dependence of gold dissolution, which reports the decomposition of cyanide in aqueous solutions with gold at temperatures above 100 °C;[42−44] however, the thermal decomposition of polymeric AuCN complexes has been reported to occur at temperatures above 350 °C.[45] Thus, it is possible that restructuring competes with the predicted decomposition mechanism in which the as-adsorbed CN/Au{111} is hydrolyzed by atmospheric water vapor.[42]

Segmentation analysis,[46−49] which takes into account all information in the images, was used to highlight the information pertaining to the ribbon orientation of the annealed CN/Au{111} system. Ribbon domains were observed to be rotationally offset from one another, separated by topologically distinct boundaries as shown in Figure 3A, a STM image of annealed CN/Au{111}. Information based on the analysis of detected Fourier modes (see Supporting Information) reveals, as shown in Figure 3B, the orientations of the different domains, identifies the domain boundaries, and detects Au{111} step edges. The measured angles between

DOI: 10.1021/jacs.6b06046
J. Am. Chem. Soc. 2016, 138, 15580−15586

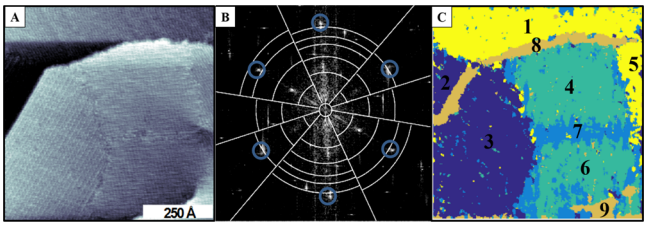

Figure 3. (A) Scanning tunneling microscope image of the annealed CN/Au{111} with six separate ribbon domains and three different relative rotations of the ribbon direction. Imaging conditions: V_{sample} = −1 V and I_{tunnel} = 5 pA. (B) Associated segmented image partitioned in the Fourier domain highlighting the three different orientations. (C) Regions 1−6 represent ribbon regions, with each color indicating a ribbon region of a different rotational orientation. Region 7 is a ribbon domain boundary, and regions 8 and 9 are step edges. Ribbon orientations are relatively offset by rotations of multiples of 60° following the hcp symmetry of the underlying gold surface.

the different ribbon domains are all calculated to be multiples of 60°, indicating that ribbon direction is significantly influenced by the hexagonal symmetry of the underlying gold substrate.

Segmentation analysis was further utilized on the molecular-resolution STM image in Figure 4A to isolate the three distinct

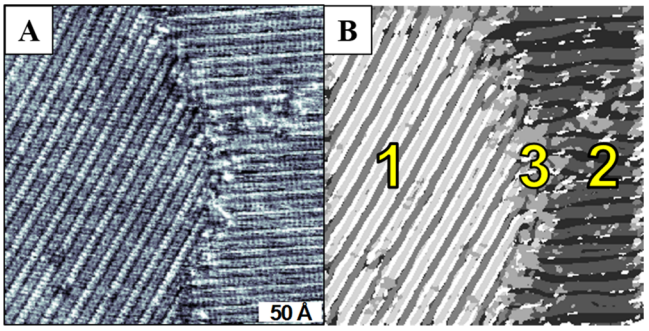

Figure 4. (A) Scanning tunneling microscope image of the region of thermally annealed CN/Au{111} with a domain boundary separating rotational domains. Imaging conditions: V_{sample} = −1 V and I_{tunnel} = 5 pA. (B) Segmentation analysis results showing the domain boundary (3) and the rotational domains (1 and 2).

regions shown in Figure 4B that compose the ribbons.[46−49] The regions identified as 1 and 2 in the segmented image are two separate ribbon regions that are offset by 120°. Region 3 is an example of a typical domain boundary between two orientation domains observed to be a topographically distinct molecular region. Within region 1, three distinct rows compose the ribbon features along with disordered portions disrupting the continuity of the ribbons. These disordered molecular regions are similar in structure to the molecules observed in the domain boundary.

Positions of the molecules within the different ribbon regions were analyzed to develop a structural model. The STM images in Figure 5, along with corresponding surface profiles, were used to generate the lattice spacing and apparent height information summarized in Table 1. Figure 5A,B shows the expected apparent height of a typical step edge on the Au{111} surface. Using this distance as an internal reference, the relative apparent height difference between two adjacent rows of the ribbons under these conditions is 0.33 ± 0.09 Å. This measurement is close to the published experimental and calculated results for the difference between Au−C and Au−N bond lengths in solid, crystalline AuCN, in which the Au−C bond is reported as longer,[50] although we do not expect STM images to yield physical height differences because they are convolutions of geometric and electronic structure.[51−54] Lateral distances for the ribbon structure are also summarized in Table 1, and correspond to letters a−f from the profiles of Figure 5C shown in Figure 5D. Note that all of the observed lateral distances are within experimental error of the lattice constant we measured for the initial as-adsorbed CN/Au{111} and take into account at least 10 independent samples using over 50 images, suggesting that the upright orientations of the molecules are maintained. This result is further supported by vibrational spectroscopic results discussed below.

The vibrational spectra were analyzed to help construct a structural model for annealed cyanide SAMs on Au{111}. The process of annealing monolayers of CN on Au{111} results in a blue shift of the frequency of the CN vibration. Cyanide molecules initially adsorbed on Au{111} at room temperature exhibit a peak at 2146 cm^{-1} as shown by attenuated total reflection infrared (ATR-IR) spectroscopy, which is in good agreement with the typical blue shift expected from the free cyanide ion in solution.[38,40,55] The Au−CN bond is typically considered to be of partially covalent character in gold−cyanide coordination complexes, with the bond strength exceeding that of Au−S.[7,13,56,57] Alkanethiol SAMs exhibit mobility on the surface,[7,58] and the same can be suggested for cyanide monolayers. After 6 h of heating at 100 °C, the spectrum of CN/Au{111} in Figure 6A shows a new peak at 2235 cm^{-1} along with the original as-adsorbed peak. The new peak is within the expected range for covalently bound CN on Au.[38,50,59] Additional heating, typically for 18 h, generates a monolayer with the spectrum shown in Figure 6B, where the original peak has disappeared. Surprisingly, the IR spectra did not contain a separate measurable peak for the weaker Au-NC bound molecules, and no other peaks were observed in regions indicating new bond formation. Breaking the CN bond and/or desorption of the CN molecules from the surface would result in complete loss of the detected vibrational mode in this region. As described below, surface-enhanced Raman spectroscopy *does* yield additional spectral features (*vide infra*).

The orientation of the cyanide molecules in the annealed system was determined through the use of polarization-modulation infrared reflection absorption spectroscopy (PM-IRRAS). The selection rules for PM-IRRAS require that only the interactions with dipoles oriented normal to the surface are detected.[60] Because of challenges due to rigidity, the thinness of the molecular layer, and specular reflection from the flatness of the Au{111}, we used polycrystalline Au/Si (as opposed to Au on mica for STM measurements) for PM-IRRAS measurements (see Supporting Information). Figure 6C shows the PM-IRRAS spectrum for annealed CN/Au{111}, for comparison with the ATR-IR spectra for the as-adsorbed and annealed cyanide monolayers. Apart from the small deviation (2 cm^{-1}) between the annealed ATR-IR and PM-IRRAS, the spectra were in good agreement, indicating that bonding interpretations based on the spectral analyses should be valid for both systems. The results indicate that, after thermal annealing, the molecules are oriented normal to the surface.

Substrate−adsorbate modes for cyanide bound to gold surfaces are found in the low-frequency region, ∼100−500 cm^{-1}, of the Raman spectrum.[50,57] The surface-enhanced Raman spectra of cyanide SAMs on Au{111} after annealing for 24 h at 100 °C are shown in Figure 7, with the typical

DOI: 10.1021/jacs.6b06046
J. Am. Chem. Soc. 2016, 138, 15580−15586

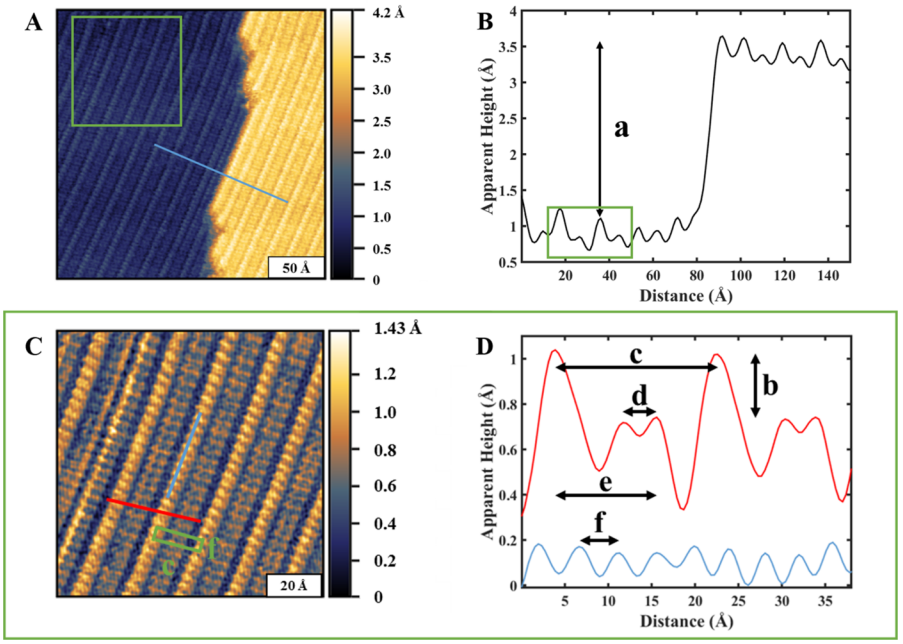

Figure 5. (A,C) Scanning tunneling microscope images of the ribbon structures of annealed CN on Au{111} (false colored to highlight the relative apparent height differences and lateral distances). The close-packed substrate lattice direction is indicated by the straight step edge and ribbon orientation in (A). (B) Surface profile shown as the blue line in (A), showing the apparent height variations of the ribbon structure of annealed CN on Au{111} and a step edge, which is used as an internal reference. (C) Higher resolution image of the area indicated in (A), with the unit cell shown as the green box. (D) Corresponding surface profiles along and across the rows shown in (B). Letters a–f correspond to the measured peak-to-peak distances summarized in Table 1. Imaging conditions: V_{sample} = −1 V and I_{tunnel} = 5 pA.

Table 1. Measured Distances for Annealed CN/Au{111} Corresponding to the Profiles Shown in Figure 5

feature	lateral distance (Å)	apparent height (Å)
a	–	2.39 ± 0.09
b	–	0.33 ± 0.09
c	18.1 ± 0.1	–
d	3.5 ± 0.4	–
e	11.5 ± 0.2	–
f	3.8 ± 0.4	–

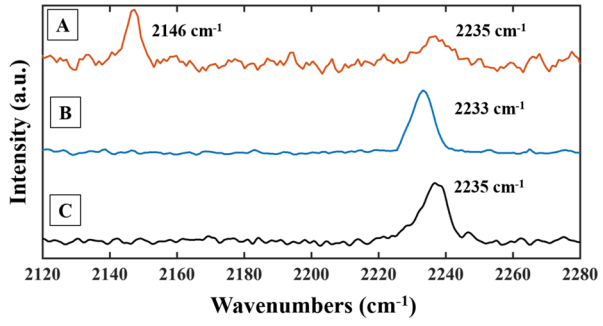

Figure 6. Attenuated total reflection infrared spectra of CN/Au{111} (A) after 6 h of thermal annealing at 100 °C and (B) after 24 h of thermal annealing at ∼100 °C. (C) Polarization-modulation infrared absorption spectroscopy for CN/Au/Si after 24 h of thermal annealing at 100 °C.

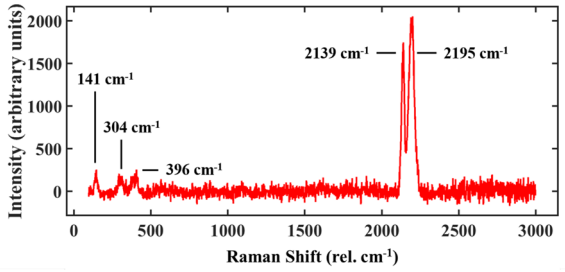

Figure 7. Raman spectrum showing both the low- and high-frequency modes of CN/Au{111} after thermal annealing for over 24 h at ∼100 °C. The most important aspects of the spectrum are the new peaks at 141 and 2195 cm^{-1} without loss of the vibrations that are also detected on the as-adsorbed sample.

vibrational modes, also observed in the as-deposited monolayers, which are known to be characteristic of Au-CN bonding. The values of 304 and 396 cm^{-1}, representing the Au-CN stretch and Au-CN bend, are red-shifted by 10 cm^{-1} in comparison to those of the initial as-adsorbed cyanide.[50,53,61,62] An additional low-frequency peak is observed at 141 cm^{-1}, close to the Au-NC vibrational frequency reported for the Au-NC containing hexagonally bundled, linear AuCN chains of the solid crystal.[50] Furthermore, a second, blue-shifted peak is observed in the region of the CN vibrational frequency at 2195 cm^{-1}, which is also close to the reported value for the same crystalline structure (see Supporting Information, Figure S6, for a comparison with the as-deposited system).[50] The appearance of the 2195 cm^{-1} vibration is an indication of Au-NC on the surface because only the "infinite" chain structure of the AuCN solid that contains the Au-NC configuration, as opposed to the solution complex, $Au(CN)_2^-$, exhibits the Au-NC vibration.[50,62]

Bonding Model for Annealed Cyanide Bonding on Au{111}. Combining the structural and vibrational characterization, we propose a bonding scheme, shown in Figure 8, to describe the annealed CN/Au{111} ribbon structure. The alternating regions of oppositely oriented molecules were constructed using the 0.33 Å difference in apparent height to

DOI: 10.1021/jacs.6b06046
J. Am. Chem. Soc. 2016, 138, 15580–15586

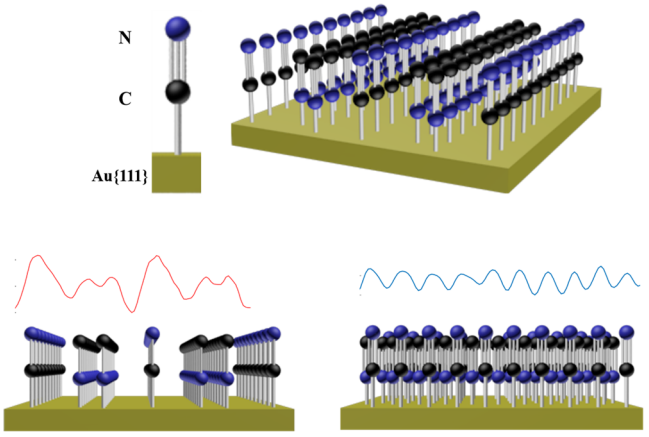

Figure 8. Proposed bonding scheme for annealed cyanide SAMs on Au{111} composed of a mixture of Au-CN and Au-NC bound molecules. Surface profiles that match the scanning tunneling microscope image shown in Figure 5 are aligned with the schematic for comparison.

match the measurement that closely matches the reported distance difference between longer Au−C and shorter Au−N bond lengths in the AuCN crystal.[50] In the annealed structure, two rows of Au-NC are separated on each side from a row of Au-CN by a single-molecule-wide vacancy row (bottom left of Figure 8). In this arrangement, the molecules maintain the pre-annealing lattice spacing[38] and match the measured unit cell, containing three molecules (3.8 Å × 18.1 Å) shown previously in Figure 5C. Note that the new structure does not maintain the hexagonal lattice of the as-adsorbed system, but the ribbon *direction* continues to follow the close-packed direction of the underlying Au{111} substrate (the straight step edges in Figure 5A).

In nitrile SAMs on Au{111}, unfavorable dipole−dipole interactions are minimized when the functional group assumes an orientation almost parallel to the substrate, enabling a tip-to-tail configuration.[1,14,63,64] This interaction is one possibility for the driving force for the transition between structures here.[63] Dipole−dipole interactions between inverted adjacent rows would be favorable after the inversion of the cyanide molecules from Au-CN to Au-NC, but the other energetics have to be considered as well. Only calculations on infinite, linear AuCN chains of the crystalline structure have reported the Au-NC vibrational frequency.[50] Also consistent with this model is the higher frequency CN vibration that is typically associated with a significantly covalent bonding environment, which is reported for gold−cyanide complexes, frequently found in nitriles, and reported for solid, crystalline AuCN.[50,55,65−67]

CONCLUSIONS AND PROSPECTS

Cyanide monolayers that are initially hexagonally close-packed when deposited at room temperature form a ribbon structure after thermal annealing for over 18 h at 100 °C on Au{111}. In this arrangement, molecules assume positions in "striped" regions that follow the hexagonal symmetry of the underlying gold substrate. Images of annealed CN/Au{111} reveal regions within the ribbons that have a relative height difference that is in agreement with calculated and experimentally determined differences between bond lengths of the longer Au-CN and shorter Au-NC bonding schemes.[50] Infrared spectroscopic measurements indicate that the CN vibration shifts from 2146 to 2233 cm^{-1} while maintaining an upright orientation. Surface-enhanced Raman spectroscopy reveals an *additional* substrate−adsorbate bonding mode that is consistent with the observed Au−N bonding mode in linear AuCN crystalline chains along with a doublet in the high-frequency region, suggesting that another chemical state exists, which we attribute to Au-NC. Ribbon regions of similar apparent height are measured in multiples of the cyanide molecule lattice constant of ∼3.8 Å. We conclude by proposing a bonding scheme consisting of a mixed monolayer of upright cyanide and isocyanide molecules on the surface that is the result of a thermally induced process crystallizing the surface, similar to what is found in solid AuCN. Such control of orientation may ultimately be of use in templating the growth of one- and two-dimensional materials on substrates.[68,69]

EXPERIMENTAL METHODS

Monolayer Preparation. Au{111}/mica substrates (150 nm of Au{111}, Agilent Technologies) were hydrogen flame annealed, as described previously, to clean the surface and to increase the size of the atomically flat terraces.[7,70] Monolayers of cyanide were prepared for STM measurements by placing 0.1 mg of solid KCN (≥96%, Sigma-Aldrich), stored in a desiccator without any further purification or treatment, in a glass vial with the Au{111}/mica substrate for 24 h at room temperature.[38]

Caution: *KCN is highly toxic and produces the volatile and flammable HCN(g) when it reacts with water and oxygen. It should be used with proper personal protective equipment, in a fume hood, and kept out of extreme temperatures.*

Afterward, the Au{111}/mica substrate was removed from the vial with the KCN, transferred to a clean glass vial in order to heat the sample only (not the KCN), and allowed to rest in the fume hood for 1 h before being placed in an oven for annealing at 100 °C for either 6, 18, or 24 h. Following annealing, the samples were allowed to cool to room temperature and placed directly into the STM for imaging without further treatment.

Scanning Tunneling Microscopy. A custom-built, Besocke-style scanning tunneling microscope was used under standard ambient conditions using custom cut Pt/Ir tips (80:20).[16,71] All STM images were calibrated against known references: Au{111} step edges for height and a decanethiol-on-Au{111} matrix for lateral distance measurements.[16] Unless otherwise specified, all samples were held at −1 V bias with a 5 pA tunneling current and image resolution of 256 × 256 pixels.

Infrared Spectroscopy. IR spectra were collected using a Thermo-Fisher Nicolet 8700 interferometer (Thermo-Fisher Scientific, Waltham, MA) and the packaged OMNIC Software (Thermo-Fisher Scientific). The OMNIC software was also used for processing the spectra and identifying peak positions. All IR samples were incubated with KCN and annealed in the same manner as described for the STM samples. The entire beam path was purged with flowing N_2, and a liquid-nitrogen-cooled mercury−cadmium−telluride detector was used to record spectra with a resolution of 2 cm^{-1}. PM-IRRAS used custom Au/Cr/Si samples with an 80° grazing incident angle. Shown in the Supporting Information (Figure S5) is the evidence that the spectral feature related to the CN bond vibrational frequency is the same on Au{111} and polycrystalline Au/Cr/Si. Silicon substrates were deposited with a 10-nm Cr adhesion layer deposited at 3 Å/s and a 100-nm-thick layer of Au also deposited also at 3 Å/s. For collecting IR spectra on Au{111}, we used custom-made Au{111}/sapphire prism substrates. Prism substrates were 0.5-cm-radius, 1-cm-high sapphire c-cut half-cylinders with a 2 nm-thick Nb adhesion layer deposited at 0.11 Å/s and a 40-nm-thick layer of Au, which is well below the optical penetration depth for metals in the range of the IR frequencies of interest, deposited at a rate of 0.5 Å/s. A bare Au{111}/sapphire prism sample was used for the background spectrum, with an incident angle $\theta = 60° > \theta_c = 34.6°$ as measured relative to the surface normal (the critical angle is calculated using $n = 1.76$). After

DOI: 10.1021/jacs.6b06046
J. Am. Chem. Soc. 2016, 138, 15580−15586

incubation and annealing, both STM and IR samples were directly analyzed without rinsing.

Raman Spectroscopy. Surface-enhanced Raman spectroscopy (SERS) was performed on a Renishaw confocal Raman microscope (Renishaw, Inc., Hoffman Estates, IL) configured with a laser at 514 nm wavelength, using WiRE 3.2 (Renishaw, Inc.) for spectral processing and analysis. Two substrates designed for surface enhancement were used in this work: Au{111}/mica with nanohole arrays and nanostructured Au on glass. The nanohole arrays (175 nm diameter, 300 nm periodicity) on Au{111}/mica were fabricated using a focused ion beam.[25] The nanostructured Au-on-glass substrates were made by evaporating 50 Å thick Au at 1 Å/s onto a glass slide and annealing at 400 °C for 24 h. All the SERS substrates were incubated with solid KCN and annealed in the same manner as the STM/IR samples.

Image Analysis. All image analyses were performed with either our custom software,[71] Gwyddion (http://gwyddion.net/), or Matlab. The segmentation utilizing the empirical wavelet transform and variational methods is described in the Supporting Information. The empirical wavelet toolbox is available online through the Mathworks file exchange, "Empirical Wavelet Toolbox".[46−48]

■ ASSOCIATED CONTENT

Supporting Information

The Supporting Information is available free of charge on the ACS Publications website at DOI: 10.1021/jacs.6b06046.

Microscopy image analysis, IR and Raman spectroscopy, and AuCN crystallographic data (PDF)

■ AUTHOR INFORMATION

Corresponding Authors

*dla3@psu.edu
*michael.zharnikov@urz.uni-heidelberg.de
*psw@cnsi.ucla.edu

ORCID

Jérôme Gilles: 0000-0002-5626-8386

Notes

The authors declare no competing financial interest.

■ ACKNOWLEDGMENTS

The authors thank the U.S. Department of Energy, grant no. DE-SC-1037004, and the W. M. Keck Foundation for support of the experimental and analytical methods used, respectively. M.Z. appreciates financial support of the German Research Foundation (DFG), grant ZH 63/14-2.

■ REFERENCES

(1) Heister, K.; Zharnikov, M.; Grunze, M.; Johansson, L. S. O.; Ulman, A. *Langmuir* **2001**, *17*, 8−11.
(2) Weiss, P. S. *Acc. Chem. Res.* **2008**, *41*, 1772−1781.
(3) Han, P.; Weiss, P. S. *Surf. Sci. Rep.* **2012**, *67*, 19−81.
(4) Pathem, B. K.; Claridge, S. A.; Zheng, Y. B.; Weiss, P. S. *Annu. Rev. Phys. Chem.* **2013**, *64*, 605−630.
(5) Abendroth, J. M.; Bushuyev, O. S.; Weiss, P. S.; Barrett, C. J. *ACS Nano* **2015**, *9*, 7746−7768.
(6) Yamada, R.; Wano, H.; Uosaki, K. *Langmuir* **2000**, *16*, 5523−5525.
(7) Love, J. C.; Estroff, L. A.; Kriebel, J. K.; Nuzzo, R. G.; Whitesides, G. M. *Chem. Rev.* **2005**, *105*, 1103−1170.
(8) Moore, A. M.; Yeganeh, S.; Yao, Y.; Claridge, S. A.; Tour, J. M.; Ratner, M. A.; Weiss, P. S. *ACS Nano* **2010**, *4*, 7630−7636.
(9) Zhang, Z.; Kim, H.; Noh, J.; Ahn, Y.; Son, J. Y.; Jang, J. *Nanoscale* **2016**, *8*, 1133−1139.
(10) Joo, S.-W.; Kim, W.-J.; Yun, W. S.; Hwang, S.; Choi, I. S. *Appl. Spectrosc.* **2004**, *58*, 218−223.
(11) Monnell, J. D.; Stapleton, J. J.; Jackiw, J. J.; Dunbar, T.; Reinerth, W. A.; Dirk, S. M.; Tour, J. M.; Allara, D. L.; Weiss, P. S. *J. Phys. Chem. B* **2004**, *108*, 9834−9841.
(12) Swanson, S. A.; McClain, R.; Lovejoy, K. S.; Alamdari, N. B.; Hamilton, J. S.; Scott, J. C. *Langmuir* **2005**, *21*, 5034−5039.
(13) Crudden, C. M.; Horton, J. H.; Ebralidze, I. I.; Zenkina, O. V.; McLean, A. B.; Drevniok, B.; She, Z.; Kraatz, H.-B.; Mosey, N. J.; Seki, T.; Keske, E. C.; Leake, J. D.; Rousina-Webb, A.; Wu, G. *Nat. Chem.* **2014**, *6*, 409−414.
(14) Ossowski, J.; Wächter, T.; Silies, L.; Kind, M.; Noworolska, A.; Blobner, F.; Gnatek, D.; Rysz, J.; Bolte, M.; Feulner, P.; Terfort, A.; Cyganik, P.; Zharnikov, M. *ACS Nano* **2015**, *9*, 4508−4526.
(15) Parikh, A. N.; Allara, D. L.; Azouz, I. B.; Rondelez, F. *J. Phys. Chem.* **1994**, *98*, 7577−7590.
(16) Bumm, L. A.; Arnold, J. J.; Charles, L. F.; Dunbar, T. D.; Allara, D. L.; Weiss, P. S. *J. Am. Chem. Soc.* **1999**, *121*, 8017−8021.
(17) Hohman, J. N.; Kim, M.; Schüpbach, B.; Kind, M.; Thomas, J. C.; Terfort, A.; Weiss, P. S. *J. Am. Chem. Soc.* **2011**, *133*, 19422−19431.
(18) Chen, D.; Sarid, D. *Phys. Rev. B: Condens. Matter Mater. Phys.* **1994**, *49*, 7612−7619.
(19) Delamarche, E.; Michel, B.; Kang, H.; Gerber, C. *Langmuir* **1994**, *10*, 4103−4108.
(20) Schönherr, H.; Feng, C.; Shovsky, A. *Langmuir* **2003**, *19*, 10843−10851.
(21) Furst, E. M. *Soft Matter* **2013**, *9*, 9039−9045.
(22) Han, P.; Akagi, K.; Federici Canova, F.; Shimizu, R.; Oguchi, H.; Shiraki, S.; Weiss, P. S.; Asao, N.; Hitosugi, T. *ACS Nano* **2015**, *9*, 12035−12044.
(23) Hoffmann, H.; Mayer, U.; Brunner, H.; Krischanitz, A. *Vib. Spectrosc.* **1995**, *8*, 151−157.
(24) Dunbar, T. D.; Cygan, M. T.; Bumm, L. A.; McCarty, G. S.; Burgin, T. P.; Reinerth, W. A.; Jones, L.; Jackiw, J. J.; Tour, J. M.; Weiss, P. S.; Allara, D. L. *J. Phys. Chem. B* **2000**, *104*, 4880−4893.
(25) Zheng, Y. B.; Payton, J. L.; Chung, C.-H.; Liu, R.; Cheunkar, S.; Pathem, B. K.; Yang, Y.; Jensen, L.; Weiss, P. S. *Nano Lett.* **2011**, *11*, 3447−3452.
(26) Jiang, N.; Foley, E. T.; Klingsporn, J. M.; Sonntag, M. D.; Valley, N. A.; Dieringer, J. A.; Seideman, T.; Schatz, G. C.; Hersam, M. C.; Van Duyne, R. P. *Nano Lett.* **2012**, *12*, 5061−5067.
(27) Stranick, S. J.; Parikh, A. N.; Tao, Y. T.; Allara, D. L.; Weiss, P. S. *J. Phys. Chem.* **1994**, *98*, 7636−7646.
(28) Poirier, G. E. *Chem. Rev.* **1997**, *97*, 1117−1128.
(29) Han, P.; Kurland, A. R.; Giordano, A. N.; Nanayakkara, S. U.; Blake, M. M.; Pochas, C. M.; Weiss, P. S. *ACS Nano* **2009**, *3*, 3115−3121.
(30) Hohman, J. N.; Zhang, P.; Morin, E. I.; Han, P.; Kim, M.; Kurland, A. R.; McClanahan, P. D.; Balema, V. P.; Weiss, P. S. *ACS Nano* **2009**, *3*, 527−536.
(31) Hostetler, M. J.; Stokes, J. J.; Murray, R. W. *Langmuir* **1996**, *12*, 3604−3612.
(32) Dubois, L. H.; Nuzzo, R. G. *Annu. Rev. Phys. Chem.* **1992**, *43*, 437−463.
(33) Allara, D. L.; Parikh, A. N.; Rondelez, F. *Langmuir* **1995**, *11*, 2357−2360.
(34) Pascual, J. I.; Jackiw, J. J.; Song, Z.; Weiss, P. S.; Conrad, H.; Rust, H. P. *Phys. Rev. Lett.* **2001**, *86*, 1050−1053.
(35) Rosenbaum, A. W.; Freedman, M. A.; Darling, S. B.; Popova, I.; Sibener, S. J. *J. Chem. Phys.* **2004**, *120*, 3880−3886.
(36) Haensch, C.; Hoeppener, S.; Schubert, U. S. *Chem. Soc. Rev.* **2010**, *39*, 2323−2334.
(37) Elliott, A. B. S.; Horvath, R.; Gordon, K. C. *Chem. Soc. Rev.* **2012**, *41*, 1929−1946.
(38) Guttentag, A. I.; Wächter, T.; Barr, K. K.; Abendroth, J. M.; Song, T.-B.; Sullivan, M. F.; Yang, Y.; Allara, D. L.; Zharnikov, M.; Weiss, P. S. *J. Phys. Chem. C* **2016**, DOI: 10.1021/acs.jpcc.6b06006.
(39) Iguchi, K. *J. Chem. Phys.* **1956**, *25*, 217−219.
(40) Keedy, C. R. *J. Chem. Educ.* **1992**, *69*, A296.

(41) Han, P.; Sykes, E. C. H.; Pearl, T. P.; Weiss, P. S. *J. Phys. Chem. A* **2003**, *107*, 8124−8129.
(42) van Deventer, J. S. J.; van der Merwe, P. F. *Thermochim. Acta* **1993**, *221*, 99−113.
(43) Cherevko, S.; Zeradjanin, A. R.; Topalov, A. A.; Keeley, G. P.; Mayrhofer, K. J. J. *J. Electrochem. Soc.* **2014**, *161*, H501−H507.
(44) Snyders, C. A.; Bradshaw, S. M.; Akdogan, G.; Eksteen, J. J. *Hydrometallurgy* **2014**, *149*, 132−142.
(45) Akhtar, M. N.; Isab, A. A.; Hassan, A. *J. Therm. Anal. Cal.* **2000**, *61*, 119−125.
(46) Gilles, J. *Trans. Sig. Proc.* **2013**, *61*, 3999−4010.
(47) Gilles, J.; Heal, K. *IJWMIP* **2014**, *12*, 1450044.
(48) Gilles, J.; Tran, G.; Osher, S. *SIAM J. Imaging Sci.* **2014**, *7*, 157−186.
(49) Bui, K.; Fauman, J.; Kes, D.; Torres, L., unpublished.
(50) Bowmaker, G. A.; Kennedy, B. J.; Reid, J. C. *Inorg. Chem.* **1998**, *37*, 3968−3974.
(51) Eigler, D. M.; Weiss, P. S.; Schweizer, E. K.; Lang, N. D. *Phys. Rev. Lett.* **1991**, *66*, 1189−1192.
(52) Bumm, L. A.; Arnold, J. J.; Cygan, M. T.; Dunbar, T. D.; Burgin, T. P.; Jones, L.; Allara, D. L.; Tour, J. M.; Weiss, P. S. *Science* **1996**, *271*, 1705−1707.
(53) Bumm, L. A.; Arnold, J. J.; Dunbar, T. D.; Allara, D. L.; Weiss, P. S. *J. Phys. Chem. B* **1999**, *103*, 8122−8127.
(54) Monnell, J. D.; Stapleton, J. J.; Dirk, S. M.; Reinerth, W. A.; Tour, J. M.; Allara, D. L.; Weiss, P. S. *J. Phys. Chem. B* **2005**, *109*, 20343−20349.
(55) Jobe, D. J.; Westaway, K. C. *Can. J. Chem.* **1993**, *71*, 1353−1361.
(56) Hakkinen, H. *Nat. Chem.* **2012**, *4*, 443−455.
(57) Beltramo, G. L.; Shubina, T. E.; Mitchell, S. J.; Koper, M. T. M. *J. Electroanal. Chem.* **2004**, *563*, 111−120.
(58) Ulman, A. *Chem. Rev.* **1996**, *96*, 1533−1554.
(59) Bernstein, M. P.; Sandford, S. A.; Allamandola, L. J. *Astrophys. J.* **1997**, *476*, 932.
(60) Buffeteau, T.; Desbat, B.; Turlet, J. M. *Appl. Spectrosc.* **1991**, *45*, 380−389.
(61) Pettinger, B.; Picardi, G.; Schuster, R.; Ertl, G. *J. Electroanal. Chem.* **2003**, *554*−*555*, 293−299.
(62) Senapati, D.; Dasary, S. S. R.; Singh, A. K.; Senapati, T.; Yu, H.; Ray, P. C. *Chem. - Eur. J.* **2011**, *17*, 8445−8451.
(63) Hautman, J.; Bareman, J. P.; Mar, W.; Klein, M. L. *J. Chem. Soc., Faraday Trans.* **1991**, *87*, 2031−2037.
(64) Frey, S.; Shaporenko, A.; Zharnikov, M.; Harder, P.; Allara, D. L. *J. Phys. Chem. B* **2003**, *107*, 7716−7725.
(65) Neelakantan, P. *Proc. Indian Acad. Sci. - Sect. A* **1964**, *60*, 422−424.
(66) Kunimatsu, K.; Seki, H.; Golden, W. G.; Gordon, J. G.; Philpott, M. R. *Langmuir* **1988**, *4*, 337−341.
(67) Wang, X.-B.; Wang, Y.-L.; Yang, J.; Xing, X.-P.; Li, J.; Wang, L.-S. *J. Am. Chem. Soc.* **2009**, *131*, 16368−16370.
(68) Bhimanapati, G. R.; Lin, Z.; Meunier, V.; Jung, Y.; Cha, J.; Das, S.; Xiao, D.; Son, Y.; Strano, M. S.; Cooper, V. R.; Liang, L.; Louie, S. G.; Ringe, E.; Zhou, W.; Kim, S. S.; Naik, R. R.; Sumpter, B. G.; Terrones, H.; Xia, F.; Wang, Y.; Zhu, J.; Akinwande, D.; Alem, N.; Schuller, J. A.; Schaak, R. E.; Terrones, M.; Robinson, J. A. *ACS Nano* **2015**, *9*, 11509−11539.
(69) Zhang, H. *ACS Nano* **2015**, *9*, 9451−9469.
(70) Porath, D.; Millo, O.; Gersten, J. I. *J. Vac. Sci. Technol., B: Microelectron. Process. Phenom.* **1996**, *14*, 30−37.
(71) Mantooth, B. A. Ph.D. Thesis, The Pennsylvania State University, University Park, PA, 2004.

DOI: 10.1021/jacs.6b06046
J. Am. Chem. Soc. 2016, 138, 15580−15586